Available on the CERN CDS information server **CMS PAS HIN-14-003**

CMS Physics Analysis Summary

Contact: cms-pag-conveners-heavyions@cern.ch 2014/05/20

Study of Z boson production in the muon decay channel in pPb collisions at $\sqrt{s_{NN}} = 5.02$ TeV

The CMS Collaboration

Abstract

The electroweak boson production is an important benchmark measurement in ultra-relativistic heavy-ion collisions which can provide constraints on the nuclear modification of parton distribution functions. In this paper the results from the proton-lead collision data taken in early 2013 are presented. The Z boson production cross section is measured in bins of the Z boson rapidity and transverse momentum and compared to theoretical predictions. The Z boson production is observed to be proportional to the number of elementary nucleon-nucleon collisions. The forward-backward ratio of the measured cross section is presented.

1 Introduction

Electroweak boson production is an important benchmark measurement in high-energy particle physics. The Z and W boson production was studied at hadron and e^+e^- colliders extensively at various collision energies. The latest measurements at the Large Hadron Collider (LHC) [1–8] are well described by higher-order perturbative quantum chromodynamics (QCD) using recent parton distribution functions (PDFs).

With its large center-of-mass energy and high luminosity, the LHC allows the study of Z and W production in heavy-ion collisions for the first time. Electroweak bosons are essentially unmodified by the hot and dense medium created in nucleus-nucleus collisions, and their leptonic decays are of particular interest since leptons pass through the medium without strong interaction. Both Z and W productions were measured by the ATLAS [9, 10] and the CMS [11–13] experiments using PbPb collision data taken in 2010 and 2011 at $\sqrt{s_{NN}} = 2.76$ TeV, confirming with a precision of about 10%, that the production cross section scales with the number of elementary nucleon-nucleon collisions.

However, in heavy-ion collisions, the production of electroweak bosons can be affected by the initial conditions of the collision. The free proton PDFs are expected to be modified for protons bound in the Pb nucleus, which together with the fact that the nucleus contains neutrons besides protons, can modify the observed cross sections compared to pp collisions. Various groups studied the nuclear modification of PDFs, and several results are available at next-to-leading order (NLO) precision in QCD [14–16]. The results are obtained by global fits to the available deep inelastic scattering and Drell-Yan data, which constrain the nuclear PDFs (nPDFs) in a limited region of parton longitudinal momentum fraction x and four-momentum transfer Q^2.

The production of Z bosons in proton-nucleus collisions at the LHC provides an opportunity to study the nPDFs in a high Q^2 and low x phase-space region that was never studied before [17]. For Z production the Q^2 is approximately given by the mass of the Z boson and the x ranges from 10^{-3} to 10^{-1} depending on the Z boson rapidity accessible by the CMS detector.

Different models estimate different amount of modifications of the Z production cross section (σ) versus rapidity (y) and transverse momentum (p_{T}) [18–22]. The rapidity distribution of Z bosons is sensitive to the parton content of the interacting nucleons. The symmetric rapidity spectrum of Z bosons in the center-of mass frame of pp collisions is modified by nuclear effects [21], that can be quantified by the forward-backward ratio:

$$R_{\mathrm{FB}}(y) = \frac{d\sigma(+y)/dy}{d\sigma(-y)/dy} \tag{1}$$

where positive rapidity values correspond to the proton-going direction. The goal of this paper is to measure the production cross section in bins of rapidity and transverse momentum of the lepton pairs to help constraining the parton content of the nucleons. The measurement is based on the pPb data taken in the beginning of 2013 and Z boson decays to muons.

2 The CMS detector

A detailed description of the CMS detector can be found elsewhere [23]. Its central feature is a superconducting solenoid with internal diameter of 6 m, providing a magnetic field of 3.8 T. Within the superconducting solenoid volume are a silicon pixel and strip tracker, a

lead tungstate crystal electromagnetic calorimeter, and a brass/scintillator hadron calorimeter. Muons are measured in gas-ionization detectors embedded in the steel return yoke outside the solenoid. Extensive forward calorimetry complements the coverage provided by these barrel and endcap detectors.

CMS uses a right-handed coordinate system, with the origin at the nominal interaction point, the x axis pointing to the center of the LHC, the y axis pointing up (perpendicular to the LHC plane), and the z axis along the anticlockwise-beam direction. The pseudorapidity is defined as $\eta = -\ln\tan\theta/2$, where θ is the polar angle measured from the positive z axis.

Muons are detected in the pseudorapidity range $|\eta| < 2.4$ using three technologies: drift tubes, cathode strip chambers, and resistive plate chambers. Matching muons to tracks measured in the silicon tracker results in a transverse momentum resolution between 1 and 10%, for transverse momentum values up to 1 TeV/c.

3 Event selection and muon reconstruction

The analysis is performed on the pPb collision data taken in the beginning of 2013 and corresponding to an integrated luminosity of (34.6 ± 1.2) nb^{-1} [24]. Due to the LHC magnet system the beam energies were 4 TeV for protons and 1.58 TeV per nucleon for lead nuclei, resulting in a center-of-mass energy per nucleon pair of $\sqrt{s_{NN}} = 5.02$ TeV. As a result of the energy difference between the colliding beams, the nucleon-nucleon center-of-mass frame is not at rest with respect to the laboratory frame. Massless particles emitted at $y_{\mathrm{c.m.}} = 0$ in the nucleon-nucleon center-of-mass frame will be detected at $y = -0.465$ (clockwise proton beam) or +0.465 (counterclockwise proton beam) in the laboratory frame. The results presented hereafter are expressed in the center-of-mass frame with the proton-going side defining the region of positive y values, to respect the usual convention of the proton fragmentation region being probed at positive rapidity. The direction of the higher energy proton beam was initially set up to be clockwise, and was then reversed splitting the data in two parts with comparable sizes. The whole data sample is referred to as pPb data.

During the data taking muon triggers were employed to select muon events online. The analysis is based on a sample triggered by requiring at least one muon with p_{T}^{μ} above 12 GeV/c. Offline selection criteria are applied to suppress and remove non-collision, beam-gas and electromagnetic collision events. Hadronic collisions were selected by requiring a coincidence of at least one energy deposit in the hadronic forward calorimeters on each side of the interaction point with at least 3 GeV total energy. Events were also required to contain at least one reconstructed primary vertex within 25 cm of the nominal interaction point along the beam axis and within 0.15 cm transverse to the beam trajectory. At least two reconstructed tracks were required to be associated with the primary vertex.

The muon candidates are reconstructed with an algorithm which utilizes information from the silicon tracker as well as from the muon system [25]. The acceptance cuts for the muons considered are $p_{\mathrm{T}}^{\mu} > 20$ GeV/c and $|\eta^{\mu}| < 2.4$ in order to assure that the trigger is on its efficiency plateau and to be within the geometrical coverage of the muon detectors.

Background muons from cosmic ray and heavy-quark semileptonic decays are rejected by requiring a set of quality cuts on each muon based on previous studies on the performance of the muon reconstruction [25]. At least one muon-chamber hit is required to be included in the global-muon track fit, and segments in at least two muon stations are required to be matched to the tracker track. To assure a good p_{T} measurement, the number of tracker layers with a

measurement is required to be at least 6, and the χ^2 over the number of degrees of freedom of the global-muon track fit is required to be less than 10. To further reject cosmic muons and muons from decays in flight the track needs at least one pixel layer with a measurement and a transverse (longitudinal) distance of closest approach of less than 2 (5) mm from the measured primary vertex.

Z candidate events were selected by requiring an opposite-charge muon pair with an invariant mass in the (60-120) GeV/c^2 range, where both muons satisfy the acceptance and quality cuts and at least one of them corresponds to the triggering signal.

4 Analysis procedure

The Z boson production cross section is calculated by counting the number of Z candidates in data, subtracting the background, correcting for acceptance and efficiency and dividing by the integrated luminosity. These components are evaluated in bins of the dimuon rapidity and p_{T} to determine the differential cross section and the forward-backward ratio. To determine the p_{T} spectrum, additional unfolding is needed to account for the finite resolution of the muon momentum measurement. In this section, these components are briefly introduced and the systematic uncertainties are summarized.

4.1 Signal extraction

The raw yield of Z bosons is determined by simply counting the number of opposite-charge muon pairs in the 60–120 GeV/c^2 mass region that fulfill the acceptance and selection requirements. The number of Z candidates found in the pPb data sample is 2183 and no events are found with more than one Z candidate. For the differential cross sections, the counting is performed in the dimuon transverse momentum or rapidity bins, where the rapidity is shifted to the center-of-mass frame.

Figure 1 shows the invariant mass distribution of the selected muon pairs from pPb data compared to PYTHIA+HIJING Monte Carlo (MC) simulation. The MC simulate the pN $\rightarrow Z \rightarrow \mu\mu$ process using the PYTHIA [26] generator (version 6.424, tune Z2) with a mixture of pp and pn interactions corresponding to pPb collisions. The detector response to each PYTHIA signal event is simulated with GEANT4 [27] and then embedded in a minimum bias pPb background event. These background events are produced with the HIJING event generator [28] and then simulated with GEANT4 as well. The signal and background events share the same generated vertex location and are boosted to have the correct rapidity distribution in the laboratory frame. The embedding is done at the level of detector hits and then the events are processed through the trigger-emulation and the event-reconstruction chain. The reconstructed longitudinal primary vertex and overall multiplicity distributions are reweighted to match the ones observed in data.

Possible background contributions to the $Z \rightarrow \mu\mu$ production are QCD multi-jet, $t\bar{t}$ and electroweak $Z \rightarrow \tau\tau$, $W + jets$, diboson (WW, WZ, ZZ) processes. Although the expected background contamination is small, a data-driven estimation is used to subtract the background contribution. For processes, where leptons result from decays involving (real or virtual) vector bosons, for every opposite-charge dimuon event, one expects two electron-muon dilepton events due to lepton universality. In the Z mass range, 64 opposite-charge electron-muon pairs are observed, which translate into 37 muon pairs once correction for the differences in electron and muon reconstruction efficiencies are taken into account. This 1.7% background is subtracted from dimuon signal events both inclusively and in bins of dilepton p_{T} and rapidity.

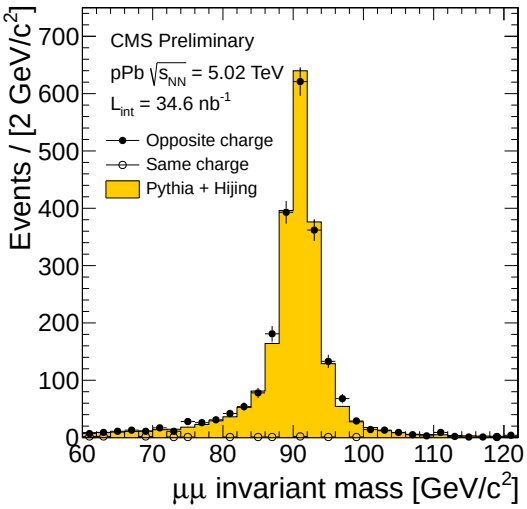

Figure 1: Invariant mass of selected muon pairs from pPb data compared to PYTHIA+HIJING simulation. The MC sample is normalized to the number of events in data – both for the 80–100 GeV/c^2 mass region.

It accounts for the main electroweak backgrounds, $t\bar{t}$ as well as the part of QCD background (such as $b\bar{b}$ decay) producing opposite-charge leptons. Remaining background, in particular from uncorrelated proton-nucleon collisions, is estimated by counting the same-charge muon pairs, which account for 0.7% background (16 candidates) in the Z boson mass range. Additional electroweak contributions from $W + jets$ and multi-boson production are found to be negligible by MC simulations.

4.2 Acceptance

The total acceptance is defined as the number of generated dimuons where both muons fulfill the acceptance cuts ($p_{\mathrm{T}}^{\mu} > 20$ GeV/c, $|\eta^{\mu}| < 2.4$) over the number of all generated dimuons in the 60–120 GeV/c^2 mass region. The baseline acceptance as a function of Z boson rapidity and transverse momentum is calculated using simulations. The event generation is provided by the POWHEG generator [29] with CT10NLO free proton PDF set [30], interfaced with PYTHIA parton shower and boosted to the laboratory frame. Final-state photon radiation (FSR) is also simulated by PYTHIA.

The total acceptance for Z production is 0.513 ± 0.024. The acceptance in bins of $y_{\mathrm{c.m.}}$ varies between 11% and 80% from the forward/backward bins to the midrapidity region and it is asymmetric in the center-of-mass frame because of the symmetric muon coverage in the laboratory frame. In order to avoid large uncertainties due to the extrapolation to regions in rapidity where the CMS detector is not suited to measure dimuons, a restricted rapidity range is also defined with dimuons measured in the $-2.5 < y_{\mathrm{c.m.}} < 1.5$ region, where the acceptance as a function of dimuon rapidity is above 40%. The acceptance correction in the restricted rapidity range is 0.703 ± 0.006 from POWHEG+PYTHIA MC sample and it varies by a few percent in bins of Z boson p_{T}.

4.3 Efficiency and resolution

The combined reconstruction, muon identification and trigger efficiency for Z bosons is defined as the number of reconstructed Z candidates, where both muons fulfill the acceptance

and selection requirements, over the number of generated Z where both muons fulfill the acceptance cuts. The efficiency is calculated from the PYTHIA+HIJING simulation samples so that the effects of the pPb environment are taken into account.

For the rapidly-falling dimuon p_{T} spectrum, an unfolding technique based on the inversion of a response matrix is first applied to the data, similar to the one used in [5], before applying the efficiency correction. This is driven by the fact that the transverse momentum resolution is not negligible compared to the analysis bin sizes. The response matrix is constructed from the PYTHIA+HIJING simulation to take into account the detector resolution effects and inverted to unfold the measured dimuon p_{T} distribution.

Using unfolding in dimuon rapidity is not needed as the shape of the y spectrum is almost flat and the resolution is a small fraction of the analysis bin size. Instead, the efficiency corrections are calculated such that to take into account the resolution effects in rapidity. The denominator is based on the number of generated dimuon events that survive the selection on kinematical quantities, whereas the numerator is based on the number of reconstructed dimuon events after applying the selection criteria to the dimuon reconstructed quantities and binning in reconstructed kinematics.

To correct for possible differences between data and simulation, a data-driven method is used to determine a correction factor to the baseline efficiency from simulation. Similar to the method described in [25], correction factors are determined by applying the *tag-and-probe* method on both data and simulation to calculate single muon efficiencies for reconstruction, identification and triggering. The ratio of each efficiency from data and simulation is then applied to reweight the simulation on a muon-by-muon basis. The overall ratio of the single muon efficiencies is consistent with unity, and the dimuon efficiency is scaled by a factor of 0.996 ± 0.017.

The overall efficiency of reconstruction, identification and trigger matching is found to be 0.901 ± 0.015 for Z candidates after taking into account the degree of agreement between simulation and data.

4.4 Systematic uncertainties

The total systematic uncertainty on the Z cross section in pPb collisions is calculated by adding in quadrature the different contributions from the raw yield after background subtraction, acceptance and efficiency determination and the unfolding technique. No other sources are found to contribute substantially.

The raw yield of Z candidates suffers from the uncertainty of the background subtraction method. The number of subtracted background events is varied by $\pm 100\%$ to assign an uncertainty on the signal extraction. The uncertainty on the inclusive yield is 1.7% from this background variation.

The uncertainty of the acceptance correction comes from the uncertainty of the theory predictions and is estimated by changing the shape of the generated rapidity and p_{T} distributions of the Z bosons to cover differences in PDFs and possible nuclear effects. The generated dimuon rapidity is varied linearly by $\pm 30\%$ in the $-3 < y_{c.m.} < 3$ range and the generated dimuon transverse momentum is varied linearly by $\pm 10\%$ in the $0 < p_{\mathrm{T}} < 150$ GeV/c range when estimating the uncertainty of the acceptance. These variations cover the predicted nuclear effects to the rapidity and p_{T} spectrum from different groups [18, 19, 21] as well as the statistical uncertainties of the present measurement. The resulting uncertainty on the total acceptance is 4.7% due to the extrapolation to the most forward and backward rapidity regions. The acceptance correction to the restricted rapidity range has an uncertainty of 0.9%.

The systematic uncertainty of the efficiency comes from two different sources. First the shapes of the underlying rapidity and transverse momentum distributions are varied with the same functions as for the acceptance resulting in a 0.2% uncertainty on the dimuon efficiency. Second the uncertainty of the correction factors from the ratio of data and simulation in the tag-and-probe method is propagated to the dimuon efficiency. The statistical uncertainties of the measured correction factors are taken into account by recomputing the dimuon efficiency multiple times using an ensemble of the single muon correction factor maps (in muon η) where the entries are modified randomly within ± 1 standard deviation of the uncertainties. In addition, the tag-and-probe technique employed carries itself an uncertainty of about 1%. Finally, the uncertainty from the three different components of the efficiency are combined in quadrature resulting in an overall uncertainty on the dimuon efficiency of 1.7%.

Table 1 summarizes the systematic uncertainties on the inclusive cross section in the full phase space and in the restricted rapidity range, together with the ranges of the relative uncertainties across the p_{T} and $y_{\mathrm{c.m.}}$ bins from the different sources. The systematic uncertainties are combined in quadrature for the final results. The integrated luminosity is calibrated by the Van der Meer scans [24] with a systematic uncertainty of 3.5%. This is the dominant systematic uncertainty of the measurement in the restricted rapidity range.

Table 1: Summary of the relative systematic uncertainties on the inclusive and differential cross sections.

Source	σ(inclusive)	$\sigma(y_{\mathrm{c.m.}} \in (-2.5, 1.5))$	$d\sigma/dp_{\mathrm{T}}$	$d\sigma/dy_{\mathrm{c.m.}}$
Acceptance	4.7%	0.9%	0.4% – 1.2%	0.1% – 1.1%
Efficiency from MC	0.2%	0.2%	0.1% – 0.3%	0.01% – 0.9%
Data/MC efficiencies	1.7%	1.7%	1.7%	1.7% – 3.4%
Background	1.7%	1.8%	0.3% – 5.4%	0.5% – 2.4%
Overall	5.3%	2.6%	2.1% – 6.3%	1.9% – 4.3%
Luminosity		3.5%		

All the uncertainties above are evaluated in bins of dimuon rapidity and p_{T} for the differential cross sections. The uncertainty of the forward-backward ratio is calculated by evaluating the variations of the background subtracted yield, the acceptance and the efficiency as described for the inclusive quantities. The combined systematic uncertainty on the forward-backward ratio ranges from 0.7% to 3.0%.

There is an additional uncertainty on the p_{T} spectrum coming from the matrix inversion procedure. The uncertainty is determined by varying the generated dimuon p_{T} distribution and the single muon p_{T} resolution. The reconstructed p_{T} distributions from PYTHIA+HIJING and POWHEG+PYTHIA as well as the weighted p_{T} spectrum accounting for possible nPDF differences were all probed and the effect on the results directly evaluated. The single muon momentum resolution was estimated from Z boson shape analysis in data and MC in different phase space regions and the largest possible difference was determined to be below 10%. Variation of this size was introduced to influence the reconstructed spectra while still applying the nominal unfolding matrix. The two sources give uncertainty of similar magnitude and the combined uncertainty on the unfolded yield is about 1.7% in the first dimuon p_{T} bin and less than 1% for higher p_{T} bins.

5 Results

In this section the results of the analysis are presented and compared to theoretical predictions. First the Z production cross section is calculated for pPb collisions then the differential cross section is presented as a function of Z boson rapidity. Also the forward-backward ratio is calculated from equation (1), since it is expected to be more sensitive to nuclear effects [21]. Finally, the differential cross section as a function of the Z boson transverse momentum is calculated and compared to theoretical predictions.

5.1 Z boson production cross section

The Z boson production cross section is calculated using the following equation:

$$\sigma = \frac{S - B}{\alpha \cdot (\epsilon \cdot \mathrm{SF}) \cdot L_{\mathrm{int}}} \tag{2}$$

where S is the number of Z candidates, B is the estimated background, α is the acceptance from POWHEG+PYTHIA simulation, $(\epsilon \cdot \mathrm{SF})$ is the efficiency from PYTHIA+HIJING simulation corrected by the data-driven scale factors from tag-and-probe method and L_{int} is the integrated luminosity.

The inclusive Z production cross section in pPb collisions calculated by equation (2) is

$$\sigma_{\mathrm{pPb}\to Z\to\mu^+\mu^-} = 134.4 \pm 2.9(\mathrm{stat.}) \pm 7.1(\mathrm{syst.}) \pm 4.7(\mathrm{lumi.})\ \mathrm{nb}. \tag{3}$$

This measurement suffers from the extrapolation of the detector acceptance to the full phase space of the Z production, which has an uncertainty of 4.7%. The prediction of the NLO calculation from POWHEG+PYTHIA gives a pp cross section at 5.02 TeV of 644 ± 32 pb for $Z \to \mu^+\mu^-$ production in the 60–120 GeV/c^2 mass range. Scaling this number by the number of nucleons in the Pb nucleus ($A = 208$), for pPb collisions one gets 134 ± 7 nb, which is consistent with the measured value. The pp theory prediction uncertainties come from missing higher order corrections and from the uncertainties in the PDF sets.

The measured cross section in the restricted $(-2.5 < y_{\mathrm{c.m.}} < 1.5)$ rapidity range is

$$\sigma_{\mathrm{pPb}\to Z\to\mu^+\mu^-}(-2.5 < y_{\mathrm{c.m.}} < 1.5) = 94.1 \pm 2.1(\mathrm{stat.}) \pm 2.4(\mathrm{syst.}) \pm 3.3(\mathrm{lumi.})\ \mathrm{nb}. \tag{4}$$

For this range, POWHEG+PYTHIA gives 94.0 ± 4.7 nb after scaling, which agrees with the measured value.

The measured cross section in the fiducial region, where both muons fulfill the acceptance cuts is

$$\sigma_{\mathrm{pPb}\to Z\to\mu^+\mu^-}(p_{\mathrm{T}}^{\mu} > 20\ \mathrm{GeV}/c, |\eta_{\mathrm{lab}}^{\mu}| < 2.4) = 68.9 \pm 1.5(\mathrm{stat.}) \pm 1.7(\mathrm{syst.}) \pm 2.4(\mathrm{lumi.})\ \mathrm{nb}. \tag{5}$$

The prediction from the POWHEG+PYTHIA generator after scaling and applying the acceptance cuts on the muons is 68.6 ± 3.4 nb, which is consistent with the measured value.

5.2 Z boson rapidity distribution

The differential cross section as a function of rapidity is calculated by the following formula:

$$\frac{d\sigma_{\mathrm{pPb}\to Z\to\mu^+\mu^-}}{dy_i} = \frac{S_i - B_i}{\alpha_i \cdot (\epsilon \cdot \mathrm{SF})_i \cdot \Delta y_i \cdot L_{\mathrm{int}}} \tag{6}$$

where the acceptance and efficiency are calculated in bins of rapidity (in the center-of-mass frame).

Figure 2 shows the differential cross section of Z bosons in pPb collisions as a function of rapidity compared to predictions from POWHEG+PYTHIA, PYTHIA and MCFM [31] generators. The PYTHIA prediction is scaled to the POWHEG+PYTHIA NLO inclusive cross section. The MCFM predictions are calculated with MSTW2008NLO [32] free proton PDF set with and without the nuclear modification from EPS09 [15] or DSSZ [14] nuclear PDF (nPDF) sets. All theory predictions are scaled by $A = 208$. The 5% theoretical uncertainty and the luminosity normalization uncertainty of 3.5% are shown as different bands on the bottom panel of Figure 2.

Note that while FSR effects are taken into account in PYTHIA, the influence on the rapidity spectrum is negligibly small.

The measured differential cross section is consistent with the theory predictions within uncertainties that are dominated entirely by the statistical uncertainty.

5.3 Forward-backward ratio

Nuclear effects are expected to modify the rapidity distribution asymmetrically and thus they can be quantified by the forward-backward ratio defined in Eq. (1). This quantity is expected to be more sensitive to nuclear effects [21] because normalization uncertainties cancel both in theory and in experiment. Figure 3 shows the measured forward-backward ratio as a function of $|y_{\mathrm{c.m.}}|$ compared to the MCFM predictions with and without the nuclear modification from EPS09 or DSSZ nPDF sets.

The PDFs with nuclear modifications come with large uncertainties which makes direct hypothesis testing not practical. On the other hand, assuming no nuclear effects leads to forward-backward ratio equal to one with no significant theoretical uncertainties. Thus we test the null hypothesis of data being compatible with this simple prediction. By constructing the χ^2 from the five data points we obtain a p-value of 0.39. Due to the large statistical uncertainties, this measurement is not able to distinguish between different nuclear PDF sets but it can constrain their uncertainties by adding new data points to the global fits in a previously unexplored region of the $Q^2 - x$ phase space.

5.4 Z boson transverse momentum spectrum

The differential cross section as a function of transverse momentum is calculated using the following equation:

$$\frac{d\sigma_{\mathrm{pPb}\to Z\to\mu^+\mu^-}}{dp_{\mathrm{T}}^i} = \frac{\sum_j R_{ij}(S_j - B_j)}{\alpha_i \cdot (\epsilon \cdot \mathrm{SF})_i \cdot \Delta p_{\mathrm{T}}^i \cdot L_{\mathrm{int}}} \tag{7}$$

where R_{ij} is the unfolding matrix determined from simulation and every component is evaluated in the restricted rapidity range ($-2.5 < y_{\mathrm{c.m.}} < 1.5$). The expected nuclear modification of

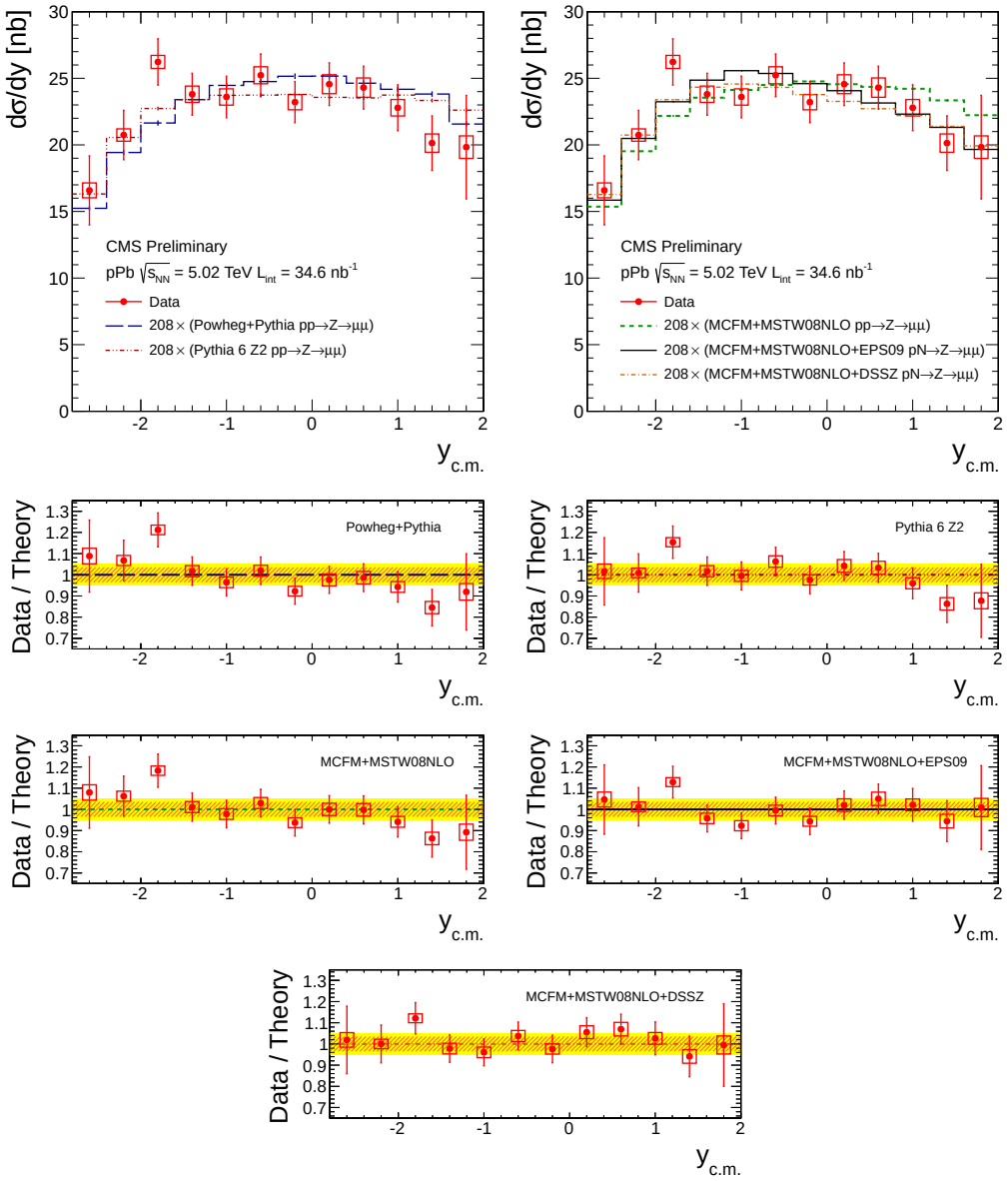

Figure 2: Differential cross section of Z bosons in pPb collisions as a function of rapidity compared to predictions from POWHEG+PYTHIA generator with CT10NLO PDF set, from PYTHIA generator with Z2 underlying event tune and from MCFM with MSTW2008NLO PDF set with and without the nuclear modification from EPS09 or DSSZ nPDF sets. All theory predictions are scaled by $A = 208$. The bottom panel shows the ratio of data and theory, where the yellow band is the theoretical uncertainty of 5% and the hashed band is the luminosity uncertainty of 3.5%, which are only shown in the ratio plots. The error bars represent the statistical, and the boxes the systematic uncertainties.

the p_{T} spectrum is small compared to the uncertainties of the theory [18, 19]. For this reason, comparisons are made only to pp theoretical predictions scaled by $A = 208$.

Figure 4 shows the differential cross section in the restricted rapidity range compared to predictions from POWHEG+PYTHIA with CT10NLO PDF and PYTHIA with tune Z2 in the same region.

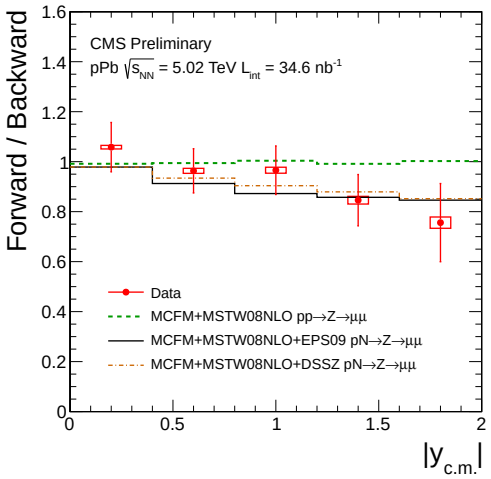

Figure 3: Forward-backward ratio of Z boson cross section in pPb collisions as a function of rapidity compared to predictions from MCFM with MSTW2008NLO free proton PDF set with and without the nuclear modification from EPS09 or DSSZ nPDF sets. The error bars represent the statistical, and the boxes the systematic uncertainties.

No deviations are found from the pp theory cross sections scaled by the number of nucleons in the Pb nucleus. The PYTHIA prediction agrees better with the measured cross section than the POWHEG+PYTHIA one, especially in the low p_{T} region where non-perturbative effects play an important role. The difference from POWHEG+PYTHIA observed in the lowest dimuon p_{T} bin is similar to the observed differences in the pp measurements at 7 or 8 TeV [2, 4, 5].

6 Summary

The Z boson production cross section has been measured in the muon decay channel in pPb collisions at $\sqrt{s_{NN}} = 5.02$ TeV. The inclusive cross sections are in agreement with NLO theoretical predictions from POWHEG+PYTHIA simulation scaled by the number of elementary nucleon-nucleon collisions. The differential cross section as a function of Z boson rapidity is consistent with the theory predictions. At large rapidity, the forward-backward ratio deviates from unity by an amount which is compatible with EPS09 and DSSZ nPDF modifications, though the statistical precision of the measurement prevents making a definitive statement. The differential cross section as a function of Z boson transverse momentum has been measured and apart from very low transverse momenta it is in fairly good agreement with the predictions from PYTHIA. The results of the presented measurement provide new data points in a previously unexplored region of phase space for constraining nuclear PDF fits.

References

[1] ATLAS Collaboration, "Measurement of the inclusive $W^{\pm}$ and Z/gamma cross sections in the electron and muon decay channels in pp collisions at $\sqrt{s} = 7$ TeV with the ATLAS detector", *Phys.Rev.* **D85** (2012) 072004, doi:10.1103/PhysRevD.85.072004, arXiv:1109.5141.

[2] ATLAS Collaboration, "Measurement of the transverse momentum distribution of Z/gamma* bosons in proton-proton collisions at $\sqrt{s} = 7$ TeV with the ATLAS detector",

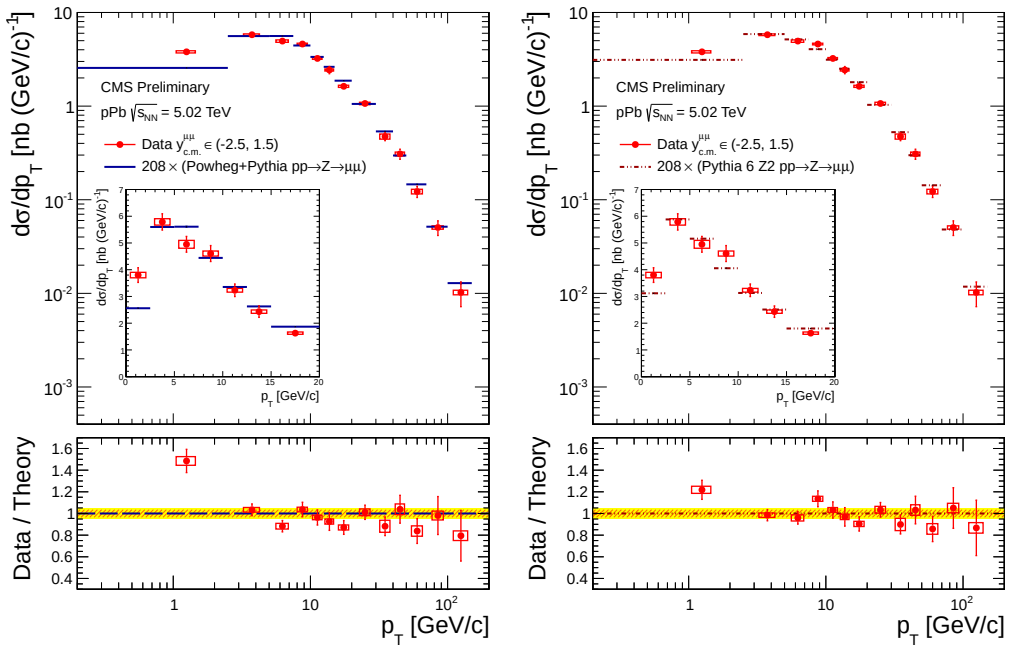

Figure 4: Differential cross section of Z bosons in pPb collisions as a function of transverse momentum in the restricted rapidity range of $-2.5 < y_{\text{c.m.}} < 1.5$ compared to predictions from POWHEG+PYTHIA with CT10NLO PDF and from PYTHIA with tune Z2. All theory predictions are scaled by $A = 208$. The bottom panel shows the ratio of data and theory, where the yellow band is the theoretical uncertainty of 5% and the hashed band is the luminosity uncertainty of 3.5%, which are only shown in the ratio plots. The error bars represent the statistical, and the boxes the systematic uncertainties.

Phys.Lett. **B705** (2011) 415, doi:10.1016/j.physletb.2011.10.018, arXiv:1107.2381.

[3] CMS Collaboration, "Measurement of inclusive W and Z boson production cross sections in pp collisions at $\sqrt{s} = 8$ TeV", *Submitted to Phys. Rev. Lett.* (2014) arXiv:1402.0923.

[4] CMS Collaboration, "Measurement of the transverse momentum distributions of Z Bosons decaying to dimuons in pp collisions at $\sqrt{s} = 8$ TeV", CMS Physics Analysis Summary CMS-PAS-SMP-12-025, 2012.

[5] CMS Collaboration, "Measurement of the Rapidity and Transverse Momentum Distributions of Z Bosons in pp Collisions at $\sqrt{s} = 7$ TeV", *Phys.Rev.* **D85** (2012) 032002, doi:10.1103/PhysRevD.85.032002, arXiv:1110.4973.

[6] CMS Collaboration, "Measurement of the Inclusive W and Z Production Cross Sections in pp Collisions at $\sqrt{s} = 7$ TeV", *JHEP* **1110** (2011) 132, doi:10.1007/JHEP10(2011)132, arXiv:1107.4789.

[7] LHCb Collaboration, "Measurement of the cross-section for $Z \to e^+e^-$ production in pp collisions at $\sqrt{s} = 7$ TeV", *JHEP* **1302** (2013) 106, doi:10.1007/JHEP02(2013)106, arXiv:1212.4620.

[8] LHCb Collaboration, "Inclusive W and Z production in the forward region at $\sqrt{s} = 7$ TeV", *JHEP* **1206** (2012) 058, doi:10.1007/JHEP06(2012)058, arXiv:1204.1620.

[9] ATLAS Collaboration, "Measurement of Z boson Production in Pb+Pb Collisions at $\sqrt{s_{NN}} = 2.76$ TeV with the ATLAS Detector", *Phys.Rev.Lett.* **110** (2013) 022301, doi:10.1103/PhysRevLett.110.022301, arXiv:1210.6486.

[10] ATLAS Collaboration, "Measurement of the $W \to \mu\nu$ charge asymmetry and centrality dependence in Pb+Pb collisions at $\sqrt{s_{NN}} = 2.76$ TeV with the ATLAS detector", ATLAS Conference Note ATLAS-CONF-2013-106, 2013.

[11] CMS Collaboration, "Study of Z boson production in PbPb collisions at nucleon-nucleon centre of mass energy $\sqrt{s_{NN}} = 2.76$ TeV", *Phys.Rev.Lett.* **106** (2011) 212301, doi:10.1103/PhysRevLett.106.212301, arXiv:1102.5435.

[12] CMS Collaboration, "Z boson production with the 2011 data in PbPb collisions", CMS Physics Analysis Summary CMS-PAS-HIN-13-004, 2013.

[13] CMS Collaboration, "Study of W boson production in PbPb and pp collisions at $\sqrt{s_{NN}} = 2.76$ TeV", *Phys.Lett.* **B715** (2012) 66, doi:10.1016/j.physletb.2012.07.025, arXiv:1205.6334.

[14] D. de Florian, R. Sassot, P. Zurita, and M. Stratmann, "Global Analysis of Nuclear Parton Distributions", *Phys.Rev.* **D85** (2012) 074028, doi:10.1103/PhysRevD.85.074028, arXiv:1112.6324.

[15] K. Eskola, H. Paukkunen, and C. Salgado, "EPS09: A New Generation of NLO and LO Nuclear Parton Distribution Functions", *JHEP* **0904** (2009) 065, doi:10.1088/1126-6708/2009/04/065, arXiv:0902.4154.

[16] M. Hirai, S. Kumano, and T.-H. Nagai, "Determination of nuclear parton distribution functions and their uncertainties in next-to-leading order", *Phys.Rev.* **C76** (2007) 065207, doi:10.1103/PhysRevC.76.065207, arXiv:0709.3038.

[17] C. A. Salgado, "The physics potential of proton-nucleus collisions at the TeV scale", *J.Phys.* **G38** (2011) 124036, doi:10.1088/0954-3899/38/12/124036, arXiv:1108.5438.

[18] V. Guzey et al., "Massive neutral gauge boson production as a probe of nuclear modifications of parton distributions at the LHC", *Eur.Phys.J.* **A49** (2013) 35, doi:10.1140/epja/i2013-13035-6, arXiv:1212.5344.

[19] Z.-B. Kang and J.-W. Qiu, "Nuclear modification of vector boson production in proton-lead collisions at the LHC", *Phys.Lett.* **B721** (2013) 277, doi:10.1016/j.physletb.2013.03.030, arXiv:1212.6541.

[20] V. Kartvelishvili, R. Kvatadze, and R. Shanidze, "On Z and Z + jet production in heavy ion collisions", *Phys.Lett.* **B356** (1995) 589, doi:10.1016/0370-2693(95)00865-I, arXiv:hep-ph/9505418.

[21] H. Paukkunen and C. A. Salgado, "Constraints for the nuclear parton distributions from Z and W production at the LHC", *JHEP* **1103** (2011) 071, doi:10.1007/JHEP03(2011)071, arXiv:1010.5392.

[22] R. Vogt, "Shadowing effects on vector boson production", *Phys.Rev.* **C64** (2001) 044901, doi:10.1103/PhysRevC.64.044901, arXiv:hep-ph/0011242.

[23] CMS Collaboration, "The CMS experiment at the CERN LHC", *JINST* **3** (2008) S08004, doi:10.1088/1748-0221/3/08/S08004.

[24] CMS Collaboration, "Luminosity Calibration for the 2013 Proton-Lead and Proton-Proton Data Taking", CMS Physics Analysis Summary CMS-PAS-LUM-13-002, 2014.

[25] CMS Collaboration, "Performance of CMS muon reconstruction in pp collision events at $\sqrt{s} = 7$ TeV", *JINST* **7** (2012) P10002, doi:10.1088/1748-0221/7/10/P10002, arXiv:1206.4071.

[26] T. Sjöstrand, S. Mrenna, and P. Skands, "PYTHIA 6.4 physics and manual", *JHEP* **05** (2006) 026, doi:10.1088/1126-6708/2006/05/026, arXiv:hep-ph/0603175.

[27] GEANT4 Collaboration, "GEANT4: A Simulation toolkit", *Nucl.Instrum.Meth.* **A506** (2003) 250, doi:10.1016/S0168-9002(03)01368-8.

[28] M. Gyulassy and X.-N. Wang, "HIJING 1.0: A Monte Carlo program for parton and particle production in high-energy hadronic and nuclear collisions", *Comput.Phys.Commun.* **83** (1994) 307, doi:10.1016/0010-4655(94)90057-4, arXiv:nucl-th/9502021.

[29] S. Alioli, P. Nason, C. Oleari, and E. Re, "NLO vector-boson production matched with shower in POWHEG", *JHEP* **0807** (2008) 060, doi:10.1088/1126-6708/2008/07/060, arXiv:0805.4802.

[30] H.-L. Lai et al., "New parton distributions for collider physics", *Phys.Rev.* **D82** (2010) 074024, doi:10.1103/PhysRevD.82.074024, arXiv:1007.2241.

[31] J. M. Campbell, R. K. Ellis, and C. Williams, "Vector boson pair production at the LHC", *JHEP* **1107** (2011) 018, doi:10.1007/JHEP07(2011)018, arXiv:1105.0020.

[32] A. Martin, W. Stirling, R. Thorne, and G. Watt, "Parton distributions for the LHC", *Eur.Phys.J.* **C63** (2009) 189, doi:10.1140/epjc/s10052-009-1072-5, arXiv:0901.0002.